Features of the middle- and low-latitude ionosphere during solar minimum as revealed from COSMIC radio occultation measurements

Libo Liu,[1,2] Huijun Le,[1] Yiding Chen,[1] Maosheng He,[1] Weixing Wan,[1] and Xinan Yue[3]

Received 25 March 2011; revised 31 May 2011; accepted 7 June 2011; published 10 September 2011.

[1] In this study, the ionospheric electron density profiles retrieved from radio occultation measurements of the Constellation Observing System for Meteorology, Ionosphere and Climate (COSMIC) mission are analyzed to determine the F_2 layer maximum electron density (N_mF_2), peak height (h_mF_2), and Chapman scale height (H_m). During the deep solar minimum of 2008–2009, N_mF_2, h_mF_2, and H_m show complicated seasonal variations, which are generally consistent with those in previous solar minima. Besides the equinoctial asymmetry, nonseasonal and semiannual anomalies are present in daytime N_mF_2; the Weddell Sea anomaly appears in nighttime N_mF_2 in all seasons except the June solstice. Unusually higher values of h_mF_2 and H_m appear at southern middle latitudes in the region centered at 70°E in the daytime and h_mF_2 at 70°W in the nighttime. Wave-like longitudinal patterns are evidently present at low latitudes in all three parameters, showing diurnal and seasonal nature. The values of the parameters under study are smaller in 2008–2009 than the rest of the COSMIC period examined in this study. The seasonal and latitudinal pattern of daytime N_mF_2 on the solar sensitivity not only confirms our earlier investigation but also explains the observed small N_mF_2 in 2008–2009 in response to the reduced solar extreme ultraviolet radiance.

Citation: Liu, L., H. Le, Y. Chen, M. He, W. Wan, and X. Yue (2011), Features of the middle- and low-latitude ionosphere during solar minimum as revealed from COSMIC radio occultation measurements, *J. Geophys. Res.*, *116*, A09307, doi:10.1029/2011JA016691.

1. Introduction

[2] Since the ionosphere is highly controlled by the variability of the solar extreme ultraviolet (EUV) radiance [*Balan et al.*, 1994; *Gorney*, 1990; *Liu et al.*, 2011b; *Richards et al.*, 1994], an interesting question is raised regarding the ionospheric state at extreme solar EUV levels [*Smithtro and Sojka*, 2005]. The ionospheric electron density (N_e) tends to linearly depend on the intensity of solar EUV at low and moderate levels [*Balan et al.*, 1994; *Gorney*, 1990] and this linear dependence for some locations and conditions breaks down at high EUV level. Under such conditions the value of N_e increases slower, remains almost constant, or even decreases with increasing EUV intensity, showing a saturation feature [*Balan et al.*, 1994; *Liu et al.*, 2006; *Liu and Chen*, 2009; *Richards et al.*, 1994]. However, N_e has recently been found to possibly increase at a higher rate with higher solar EUV intensity, which is called an amplification pattern [*Chen et al.*, 2008; *Liu and Chen*, 2009; *Liu et al.*, 2009a]. In addition, if the solar EUV dependence of total electron content (TEC) at low and moderate solar activities is directly applied to the case of very low solar EUV levels, the extrapolation for that case will give negative values of TEC [*Liu et al.*, 2009a]. This suggests that the ionosphere should act in a different way to keep nonnegative TEC in extreme solar minimum. Note that the TEC includes electrons of the plasmasphere, and the EUV dependences may be different in the ionosphere and the plasmasphere.

[3] The solar activity during 2008–2009 is extremely prolonged low among recent several solar cycles, which has attracted the interest of the space physics community [e.g., *Araujo-Pradere et al.*, 2011; *Chen et al.*, 2011; *Emmert et al.*, 2010; *Gibson et al.*, 2009; *Heelis et al.*, 2009; *Liu et al.*, 2011a; *Lühr and Xiong*, 2010; *Russell et al.*, 2010; *Solomon et al.*, 2010]. *Gibson et al.* [2009] characterized the three-dimensional solar-heliospheric-geospace system at this solar minimum and found that significant variations may occur within and between solar minima. *Russell et al.* [2010] examined how unprecedented this solar minimum might be and pointed out that the solar minimum is making us questioning our basic understanding of the solar-terrestrial physics.

[4] The deep solar minimum of 2008–2009 also offers us a unique opportunity to explore the response of the ionosphere and thermosphere under extremely low EUV conditions. By

[1]Beijing National Observatory of Space Environment, Institute of Geology and Geophysics, Chinese Academy of Sciences, Beijing, China.

[2]Also at State Key Laboratory of Space Weather, Center for Space Science and Applied Research, Chinese Academy of Sciences, Beijing, China.

[3]COSMIC Program Office, University Corporation for Atmospheric Research, Boulder, Colorado USA.

0148-0227/11/2011JA016691

analyzing global ionosonde measurements and TEC maps produced by the Jet Propulsion Laboratory (JPL), *Liu et al.* [2011a] detected smaller values in the global mean TEC, in the F_2 layer maximum electron density (N_mF_2) and in the base height of the *F* layer (as indicated by the *F* layer virtual height, h′F) during the period of 2008–2009, comparing to previous solar minima. Unfortunately, the ionosonde results provided a poor latitudinal coverage, owing to only about 30 stations available with long enough data series for the comparisons between solar cycles. Although the solar index $F_{10.7}$ fails to reliably present the solar EUV intensity during this unusual period [*Chen et al.*, 2011], the lower values of N_mF_2 and TEC in 2008–2009 can be reasonably explained by the decrease in solar EUV intensity, which was continuously monitored by Solar and Heliospheric Observatory/Solar EUV Monitor (SOHO/SEM) since the end of 1995.

[5] Furthermore, it was found that the ionospheric empirical models overestimated the satellite observations of the upper transition height, the topside ionosphere ion temperature and N_e in 2008 [*Heelis et al.*, 2009; *Lühr and Xiong*, 2010]. *Lühr and Xiong* [2010] showed that the International Reference Ionosphere (IRI) 2007 model [*Bilitza and Reinisch*, 2008] overestimated the N_e observations by 50% and more than 60% in 2008 and 2009, respectively. In contrast, the models reasonably predicted the satellite observations during other periods. *Lühr and Xiong* [2010] suggested that during the deep solar minimum of 2008–2009 the ionosphere might have exhibited different physical characteristics from the previous solar minima. The upper atmosphere becomes thinner and cooler, reaching a record-low level in 2008–2009 [*Emmert et al.*, 2010; *Solomon et al.*, 2010]. The thermospheric mass density at 400 km altitude was low by about 30% in 2008–2009. Simulated results implied that the decline in solar EUV during this period is the primary contributor to the upper atmospheric cooling. In contrast, the greenhouse gases such as CO_2 only play a secondary role in this unusual change [*Solomon et al.*, 2010].

[6] However, *Lean et al.* [2011] proposed that the associated anomalously low EUV irradiance in 2008 minimum is unlikely to be real. They used TEC data prior to 1998 from the Center for Orbit Determination in Europe (CODE) database and constructed a mean TEC database since 1998 from maps produced at four Global Positioning System (GPS) analysis centers: CODE, at the University of Berne, Switzerland; the European Space Operations Centre Ionosphere Monitoring Facility in Darmstadt, Germany; the Ionospheric and Atmospheric Remote Sensing Group at JPL, Pasadena, USA; and the Research Group of Astronomy and Geomatics, Technical University of Catalonia (UPC) in Spain. Based on the composite data series, they detected a positive trend in the daily averaged global TEC. Note that, prior to 1998, the GPS receivers are sparse and have a poor global distribution; so, the data consistency and its influence on the TEC trend needs further validation.

[7] With the advent of the ionospheric radio occultation (IRO) technique applied in satellite constellations like the Constellation Observing System for Meteorology, Ionosphere and Climate (COSMIC), improved spatial coverage along with altitude information can be achieved in monitoring the global ionosphere. The COSMIC mission registered about 1000–2500 IRO events daily, which have been used to investigate the ionosphere on various issues [e.g., *He et al.*, 2009; *Lin et al.*, 2007; *Liu et al.*, 2008, 2009b, 2010; *Luan et al.*, 2008; *Potula et al.*, 2011; *Yue et al.*, 2010b; *Zeng et al.*, 2008]. For example, *Lin et al.* [2007] studied the longitudinal structure in the equatorial ionosphere using the observations during September and October 2006. *Zeng et al.* [2008] reported that the average NmF2 during December solstice are higher than those during June solstice 2006, which is well reproduced by numerical simulations using the Thermosphere-Ionosphere Electrodynamics Global Circulation Model (TIEGCM). *Luan et al.* [2008] used the COSMIC IRO N_e profiles from November 2006 to February 2007 to study the ionospheric nighttime N_e enhancements. The evident N_mF_2 enhancements they found show different characteristics in different regions. Comparing ionospheric parameters between COSMIC observations in 2007 and IRI model predictions, *Potula et al.* [2011] suggested that the IRI model should be updated to better characterize the topside N_e profile. *Liu et al.* [2008] made an investigation of altitudinal dependence for the annual and semiannual components of the daytime N_e in the altitude range of 200–560 km. Pronounced semiannual component is found in low altitude N_e in far-from-pole (high latitudes in the East Asian and South Atlantic sectors) and equatorial regions, and the annual component tends to have maxima in local summer months at higher altitudes.

[8] The current analysis will focus on the features of the middle and low latitude ionosphere during the recent deep solar minimum. Five years of N_e profiles retrieved from COSMIC IRO measurements are collected to quantify the features of the derived ionospheric key parameters; N_mF_2, the F_2 layer peak height h_mF_2 and Chapman scale height H_m. The three parameters show seasonal pattern and longitude structure during the recent solar minimum. A salient feature is that strong wave-like patterns are simultaneously presented in daytime N_mF_2, h_mF_2 and H_m in equatorial regions, showing diurnal and seasonal nature. It is the first time to report the wave-like pattern in equatorial H_m. Another aim of this study is to elucidate the possible solar EUV effects on the three parameters, by quantifying the differences between those in 2008–2009 and the rest of the COSMIC mission period. We find a reduction in the values of the three parameters at middle and low latitudes during daytime in 2008–2009, of the order of 10^4 to 10^5 electrons/cm^3 in N_mF_2, 5–28 km in h_mF_2 and 3–8 km in H_m, accompanied with a decrease of about 6.6 solar flux units ((sfu) 1 sfu = 10^{-22} W m^{-2} Hz^{-1}) in solar 10.7 cm radio flux.

2. Data Source and Processing

[9] COSMIC is a joint Taiwan-U.S. mission, consisting of six microsatellites. These satellites, launched simultaneously in April, 2006 to an initial altitude of 500 km, now operate at altitudes around 800 km in near circular Low Earth Orbit with a 72° inclination and 30°separation in longitude from each other. The raw IRO observations are processed in both near real time and postprocess mode and stored at the COSMIC Data Analysis and Archive Center (CDAAC). N_e profiles are retrieved from the COSMIC IRO measurements via an Abel transform of slant TEC measurements. Up to now, more than 2,700,000 N_e profiles are accumulated and archived at CDAAC. These N_e profiles provide a massive database of N_e with global coverage and have attracted the interest of the

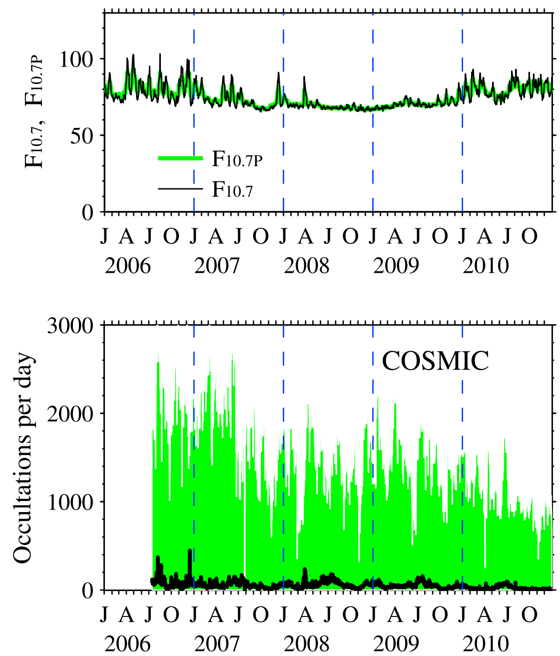

Figure 1. (top) Solar 10.7 cm radio flux index $F_{10.7}$ and an effective index $F_{10.7P}$. Here $F_{10.7P} = (F_{10.7} + F_{10.7A})/2$; $F_{10.7A}$ is the 81 day centered mean of $F_{10.7}$. $F_{10.7}$ and $F_{10.7P}$ are in solar flux unit ((sfu) 1 sfu = 10^{-22} W m^{-2} Hz^{-1}). (bottom) Shaded area in green color shows the daily number of ionospheric radio occultation events registered by COSMIC mission during 2006–2010. The black curve indicates the daily number of electron density profiles being discarded in our analysis.

ionospheric physics community to explore issues related with ionospheric climatology and specified events [e.g., *He et al.*, 2009; *Lin et al.*, 2007; *Liu et al.*, 2008, 2009b, 2010; *Luan et al.*, 2008; *Potula et al.*, 2011; *Yue et al.*, 2010b; *Zeng et al.*, 2008].

[10] The inversion process of CDAAC Abel transform introduced systemic biases in IRO N_e profiles at low latitudes and low altitudes. An error analysis by *Yue et al.* [2010a] showed that the absolute (and relative) standard deviations of the differences between the retrieved and true values are 3.2×10^{10} m^{-3} (16%) and 1.4×10^{11} m^{-3} (15%) of N_mF_2, and 8.9 km (2%) and 7.4 km (2%) of h_mF_2, nighttime and daytime, respectively. Their evaluation indicated that the retrieved N_mF_2 and h_mF_2 are generally in good agreement with the true values, but the reliability of the retrieved electron density degrades at low altitudes.

[11] The COSMIC mission during the period of 2006–2010 covers a period of low solar activity, as indicated by $F_{10.7}$ and $F_{10.7P}$ in Figure 1 (top). Here $F_{10.7P}$ is the mean value of solar 10.7 cm radio flux index $F_{10.7}$ and its 81 day centered mean $F_{10.7A}$. The reader is recommended to refer *Richards et al.* [1994] and *Liu et al.* [2006] for detailed information of $F_{10.7P}$ and the comparison of solar EUV with different solar proxies. The advantage of $F_{10.7P}$ as a solar proxy is that it linearly described the intensity of solar EUV fluxes. During the period of the COSMIC mission, geomagnetic conditions were generally quiet, and magnetic storms seldom occurred; therefore, the geomagnetic disturbance effects are ignored in our statistical analyses.

[12] Figure 1 (bottom) plots the daily number of COSMIC IRO N_e profiles used in this analysis. We collected the COSMIC IRO N_e profiles during the period from DOY (day of year) 194, 2006 to DOY 365, 2010 to deduce N_mF_2, h_mF_2 and H_m. To determine the three parameters, all COSMIC N_e profiles within the altitude range of 170–600 km are fitted one by one with a least squares procedure using an α-Chapman profile function [*Rishbeth and Garriott*, 1969]:

$$N_e(h) = N_mF_2 \exp\left\{\frac{1}{2}[1 - z - \exp(-z)]\right\}, \quad z = (h - h_mF_2)/H(h). \tag{1}$$

Here h_mF_2 is the peak height, and H(h) is the effective scale height at altitude h. We assume $H(h) = H_m + B_1 (h - h_mF_2)$, for the bottomside; and $H(h) = H_m + B_2 (h - h_mF_2)$, for the topside. H_m is the value of H(h) at h_mF_2 and B_1 and B_2 are coefficients. This fitting technique has been described by *Liu et al.* [2007, 2008, 2009b, 2010] in analyzing N_e profiles from the incoherent scatter radar observations and IRO measurements.

[13] We discarded some problematic IRO N_e profiles, which meet any of the following cases, even though some of these N_e profiles are possibly valid and real. The cases are (1) data points of a N_e profile are rather spread, possibly due to complex ionospheric structures or rather low signal-to-noise ratio of received GPS signals; (2) N_e profile distorted significantly, especially when many peaks appeared in F layer altitude range; (3) the fitted peak parameters are evidently invalid or unphysical. The first and second case will cause a fail in profile fitting by a Chapman function. This is equivalent to the mean deviation (MD) criteria of *Potula et al.* [2011]. Data points in case (3) are treated as outliers, provided their values surpass 2.5 times standard deviations out of the mean values. The daily number of these discarded profiles during the period under study is also plotted in the black line in Figure 1 (bottom). As shown in Figure 1, questionable profiles are 3–5% of the total profiles; so, the average results are less affected by questionable profiles, even if no quality control is taken.

[14] To study the possible solar EUV-generated effect on the three parameters during the recent deep solar minimum, we bin the data (h_mF_2, N_mF_2 and H_m) into two groups. Group A contains those during 2008 through 2009, and Group B for the rest (specifically, the data during the period of 2006 through 2007 and in 2010). The mean values of $F_{10.7}$ and $F_{10.7P}$ for the two groups and their seasonal differences are given in Table 1. We can see that the mean values of $F_{10.7}$ and $F_{10.7P}$ during the periods of group A are about 70 sfu, lower than those of group B by around 6.6 sfu. The solar EUV difference between the two groups (groups A and B) gives us an opportunity to quantify the solar EUV effects on the ionosphere during solar minimum.

[15] We further sort the data by season and location in each group. The globe is zoned into grids at every 5° latitudes from 70°S to 70°N and at every 10° longitudes from 180°W to 180°E. Data within ±40 days around the March Equinox, June Solstice, September Equinox and December Solstice are designated as the four seasons. For a specific season, all the

Table 1. The Mean Values of $F_{10.7}$ and $F_{10.7P}$ in 80 Days During Four Seasons for the Two Groups[a]

Season	$F_{10.7}$ ($F_{10.7P}$) for Group A (2008–2009)	$F_{10.7}$ ($F_{10.7P}$) for Group B (2006.194–365, 2007, 2010)	Difference of $F_{10.7}$ ($F_{10.7P}$) Between Two Groups
March equinox	70.0556 (70.0907)	76.5938 (76.7496)	6.5383 (6.6589)
June solstice	69.7753 (69.6726)	75.9683 (76.2724)	6.1930 (6.5998)
September equinox	69.4222 (69.3877)	75.7004 (75.9915)	6.2782 (6.6038)
December solstice	70.1301 (70.2494)	79.1071 (78.7868)	8.9770 (8.5374)

[a]Numbers in parentheses are the corresponding values of $F_{10.7P}$. Both $F_{10.7}$ and $F_{10.7P}$ are in solar flux units (1 sfu = 10^{-22} W m^{-2} Hz^{-1}).

data points in each grid are collected to do a Fourier harmonic fitting as function of local time (LT). As shown in Figure 2, the LT dependent average of N_mF_2, h_mF_2 and H_m at 60° apex latitude is reasonably described by a superposition of 4 order Fourier harmonic functions. The advantage of this Fourier harmonic fitting is to eliminate the influence of nonuniform distribution of data points with local time. This fitting technique has been applied in the investigation of the ionospheric nighttime enhancements by *Luan et al.* [2008]. The fitting procedure can determine the average values of the parameters at specified LT (0–24). In the following section, we take the values at 13 LT and 01 LT as a representation for daytime and nighttime, respectively.

3. Results

3.1. Features of N_mF_2, h_mF_2, and H_m During 2008–2009

[16] The seasonal distributions of N_mF_2 at 01 LT and 13 LT during 2008–2009 are illustrated in Figure 3, respectively. The white line superimposed on each panel of Figure 3 shows the location of the dip equator.

[17] We can see from Figure 3 that the daytime N_mF_2 during 2008–2009 show significant seasonal variations, which are outlined below:

[18] 1. The daytime N_mF_2 is highest in March Equinox compared to the rest three seasons around the equatorial anomaly crests. The seasonal pattern of N_mF_2 peaks in equinoxes, which is called the semiannual anomaly [*Torr and Torr*, 1973; *Rishbeth*, 1998; and references therein].

[19] 2. N_mF_2 is obviously higher in March Equinox than in September Equinox, which is known as equinoctial asymmetry [*Balan et al.*, 2000; *Kawamura et al.*, 2002; *Liu et al.*, 2010]. The equinoctial asymmetry is strongest over equatorial anomaly crest regions. *Balan et al.* [2000] summarized equinoctial asymmetries in the ionosphere and thermosphere with measurements of the Japanese middle and upper atmosphere (MU) radar at Shigaraki (35°N, 136°E). *Kawamura et al.* [2002] explained the observed equinoctial asymmetries over the MU radar location through the difference in the lasting time of wind directions. However, the equinoctial asymmetrical pattern of the COSMIC h_mF_2 is not totally consistent with that of N_mF_2 in both hemispheres [*Liu et al.*, 2010]. Therefore, the effect of neutral winds solely is not enough to explain the observed equinoctial features.

[20] 3. Taking the southern and northern hemispheres together, stronger daytime N_mF_2 appears in December Solstice than in June Solstice, known as nonseasonal anomaly, or annual anomaly [*Mendillo et al.*, 2005; *Rishbeth*, 1998; *Torr and Torr*, 1973; *Zeng et al.*, 2008].

[21] 4. Daytime N_mF_2 is higher in summer than in winter over most regions. The winter/seasonal anomaly (greater values of electron density in winter than in summer) [e.g., *Duncan*, 1969; *Mayr and Mahajan*, 1971; *Rüster and King*, 1973; *Torr and Torr*, 1973; *Wright*, 1963] appears only in some northern low latitude and southern equatorial regions. Thus, N_mF_2 winter anomaly subsides during this deep solar minimum. In contrast, the winter anomaly is notably during solar maximum [*Torr and Torr*, 1973].

[22] The seasonal patterns of the ionosphere have been explained by chemical and dynamic processes through changes in solar zenith angle, thermospheric composition and global circulations. *Wright* [1963] realized the linkage between the variation of daytime N_mF_2 and the upper atmospheric compositions. *Duncan* [1969] proposed an explanation

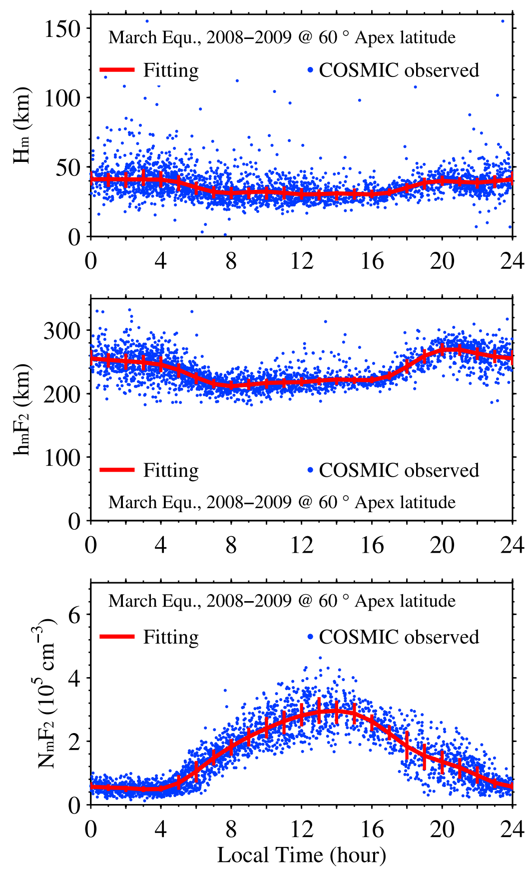

Figure 2. Local time variation of the F_2 layer (top) Chapman scale height H_m at 60° apex latitude, (middle) peak height h_mF_2, and (bottom) maximum electron density N_mF_2 during March equinox in 2008–2009. The dots denote the observed data, red vertical bars are the hourly lower and upper quartiles, and the red curve shows the fitting of the observed data with 4 order Fourier harmonic components.

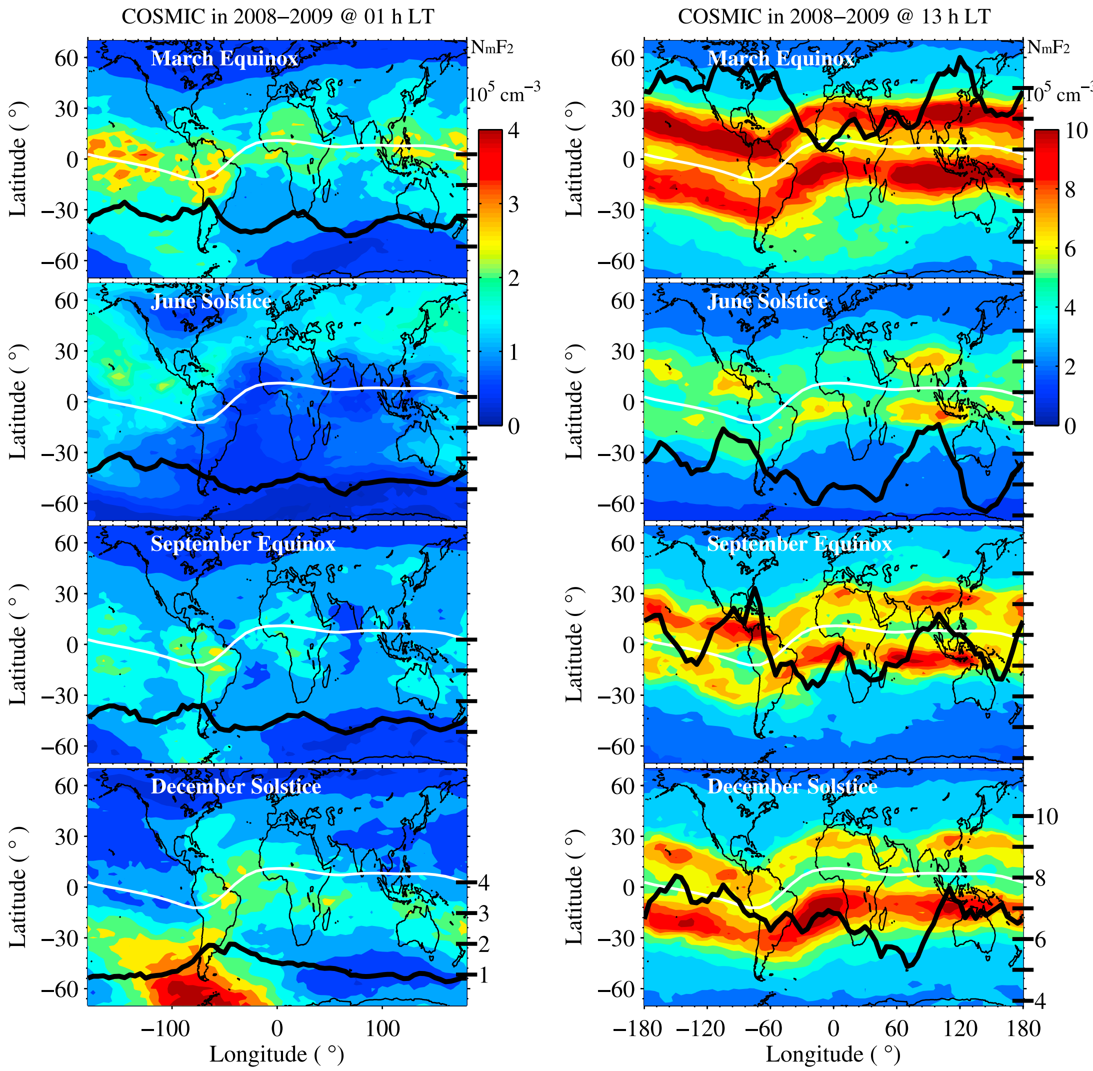

Figure 3. Spatial distribution of the F_2 layer maximum electron density N_mF_2 in four seasons in 2008–2009 at (left) 0100 LT and (right) 1300 LT. The white curve in each panel denotes the dip equator, and the black curve illustrates the longitudinal structure of the mean N_mF_2 over the 10°–25° latitude band northward of the dip equator. The right-hand horizontal bars scale the black curves.

of the winter anomaly in terms of changes in the atomic oxygen to molecular nitrogen ratio, [O]/[N_2]. *Rishbeth* [1998] made a detailed discussion on the physical processes of seasonal variations in the ionosphere. However, the annual anomaly remains an arguable topic. The TIEGCM simulations carried out by *Zeng et al.* [2008] showed that changes in solar EUV radiation between the December and June solstices and the displacement of the geomagnetic axis from the geographic axis are the two primary processes causing the annual asymmetry and its associated longitudinal and local time variations.

[23] Regarding the spatial distribution of N_mF_2, N_mF_2 in four seasons is primarily regulated by the configuration of the geomagnetic field. N_mF_2 is organized by dip contour lines such as the dip equator. This geomagnetic field controlling feature is more remarkable in the daytime. As a result, the seasonal components (the yearly mean, annual and semiannual components) are regularly distributed along dip contour lines [*Liu et al.*, 2009b]. In the daytime N_mF_2 shows a minimum near the dip equator flanked by two maxima at low latitudes on both sides, often referred to as the equatorial ionization anomaly (EIA) [*Moffett*, 1979].

[24] Besides the EIA, a salient structure is the Weddell Sea anomaly [*Burns et al.*, 2008; *He et al.*, 2009; *Horvath and Essex*, 2003; *Penndorf*, 1965]. It is a nighttime phenomenon named by *Penndorf* [1965] who found that the F_2 layer critical frequency peaks at 04 UT from the Falkland Islands (52°S, 60°W) to the southern shore of the Weddell Sea (around 75°S, 30°W). The Weddell Sea anomaly is strongest in December Solstice. Comparing the daytime with nighttime panels, we can find the nighttime enhancement in summer N_mF_2 at higher northern middle latitudes over a wider range of longitudes (100°E to 150°W) [*Burns et al.*, 2008; *Luan et al.*, 2008] and the Weddell Sea anomaly in all seasons, except during June Solstice. *He et al.* [2009] proposed an explanation of the nighttime enhancement in summer N_mF_2 over both regions in terms of the evolution of thermospheric neutral winds and the geometry of the magnetic field. The

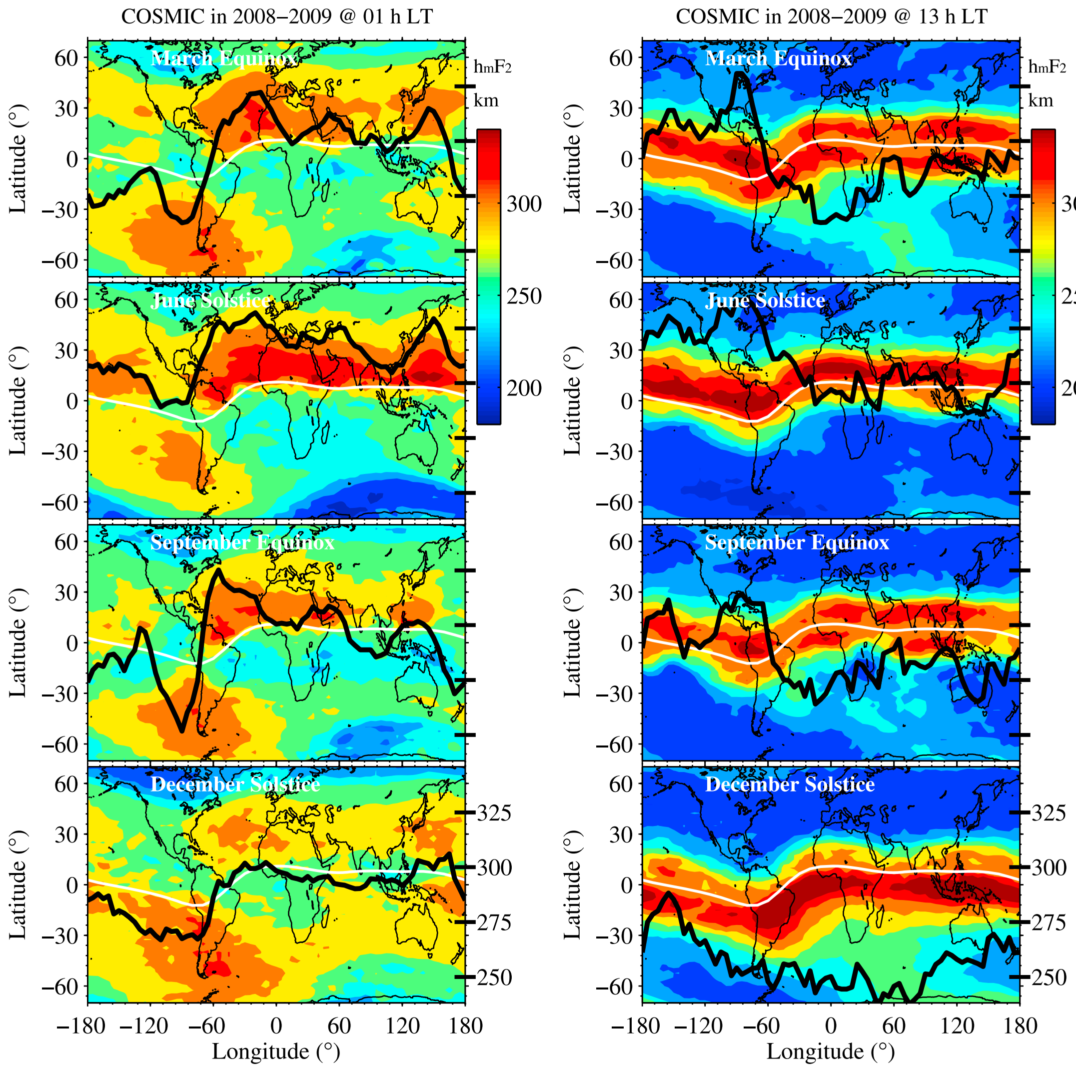

Figure 4. Spatial distribution of the F_2 layer peak height h_mF_2 in four seasons in 2008–2009 at (left) 0100 LT and (right) 1300 LT. The white curve in each panel denotes the dip equator, and the black curve illustrates the longitudinal structure of the h_mF_2 averaged over the 10°–25° latitude band northward of the dip equator. The right-hand horizontal bars scale the black curves.

enhancement in N_mF_2 and increase in h_mF_2 could arise from the thermospheric wind effect over regions with specified geomagnetic field configuration, and solar photoionization plays a crucial role in the enhancement as well [*He et al.*, 2009]. Additionally, the daytime N_mF_2 shows higher values at middle and high latitudes over the longitude sector from 60°W to 60°E during the March Equinox, compared to other seasons.

[25] Similar to N_mF_2 in Figure 3, the distributions of h_mF_2 and H_m are plotted in Figure 4 and Figure 5, respectively.

[26] We can see from Figure 4 that the distribution of daytime h_mF_2 also tends to be regulated by the geomagnetic field configuration. h_mF_2 in solstices exhibits higher values in the summer hemisphere. The hemispheric asymmetry in daytime h_mF_2 reflects the difference in the thermal structure and ionospheric dynamics, especially the hemispheric asymmetry in neutral winds and temperature [*Rishbeth*, 1998]. *Luan and Solomon* [2008] derived the meridional winds from COSMIC IRO measurements. The hemispheric asymmetric neutral winds, especially the transequatorial winds, will move the plasma across the equator to the opposite hemisphere, causing a hemispheric asymmetry in equatorial h_mF_2 in solstices [*Rishbeth*, 1998; *Luan and Solomon*, 2008].

[27] Compared to other longitudes, higher h_mF_2 extends southeastward in the southern middle and high latitude regions centered at longitude 70°E, which is most notable in the daytime of December Solstice and March Equinox (Figure 4 (right)). The spatial distribution of h_mF_2 differs in the nighttime. In the nighttime higher h_mF_2 appears at northern low latitudes in all seasons, weaker in December solstice. Higher h_mF_2 also exists in the southern hemisphere around the Weddell Sea anomaly region. Interestingly, the daytime higher values in h_mF_2 east-southward extending around 60°E are taken over by low values in the nighttime, while in the Weddell Sea anomaly region the daytime lower values turn back to higher values at night.

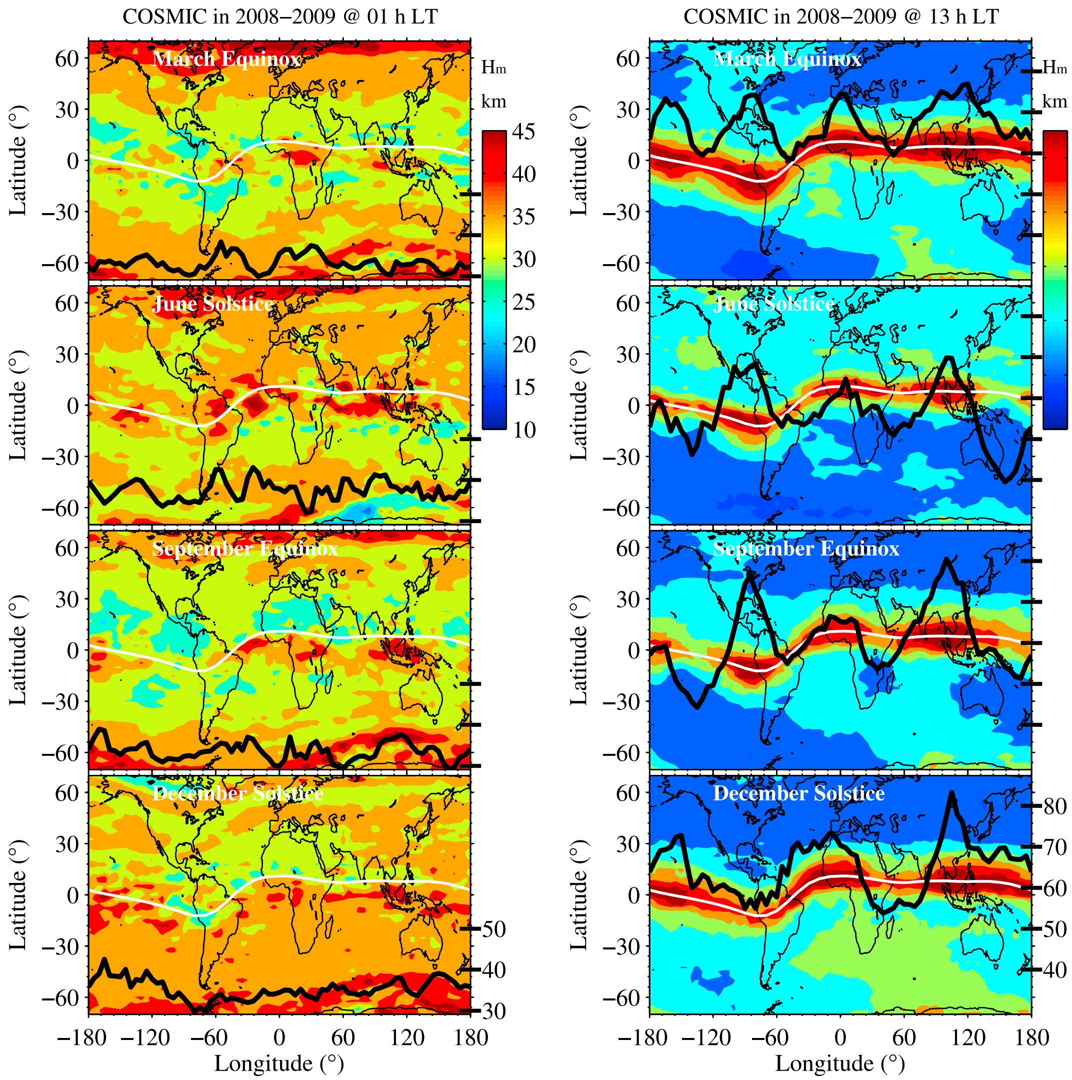

Figure 5. Spatial distribution of the Chapman scale height H_m in four seasons in 2008–2009 at (left) 0100 LT and (right) 1300 LT. The white curve in each panel denotes the dip equator, and the black curve illustrates the longitudinal structure of the H_m averaged over a latitude band ±8° around the dip equator. The right-hand horizontal bars scale the black curves.

[28] Different from that of N_mF_2, the seasonal variation in daytime h_mF_2 is simple, dominated by an annual variation peaking in local summer [*Liu et al.*, 2009b]. Through an analysis of several annual components in h_mF_2 during the earlier phase of the COMIC mission, *Liu et al.* [2009b] found that the distribution of the annual phase of daytime h_mF_2 is regulated by the dip equator.

[29] Similar to h_mF_2, the equatorial H_m in the daytime is also well regulated by the dip equator. In equatorial regions H_m has higher values in the daytime than at night, while it reverses at higher latitudes. This local time and seasonal nature of H_m is consistent with those of the vertical scale height (VSH) at 400 km [*Liu et al.*, 2008]. *Liu et al.* [2008] studied the behavior of the VSH at 400 km using the early phase COSMIC data. Please note that the daytime H_m at southern middle latitudes in the region centered at 70°E differs from that in the other longitudinal sectors. No previously published articles reported such salient structures in H_m. Additionally, the latitude pattern of daytime H_m is different from that of VSH. Besides the equatorial peak, the increase with latitude of middle latitude VSH [*Liu et al.*, 2008] is not found in daytime H_m.

[30] In literatures, the scale heights have at least three definitions, the plasma scale height, VSH and H_m [*Liu et al.*, 2007]. The plasma scale height (H_p) is defined as $H_p = k_b (T_i + T_e)/m_i g$, where k_b is the Boltzmann constant, g is the acceleration due to gravity, m_i is the mass of ions, T_i is ion temperature and T_e is electron temperature. VSH defined as the value of $-dh/d(\ln(N_e))$, is related to the gradient of the N_e profile [*Kutiev et al.*, 2006]. The inherent relationship among H_p, H_m and VSH retrieved from ISR measurements at Arecibo (114.4°E, 30.6°N), Puerto Rico has been investigated by *Liu et al.* [2007], which provided evidences that both the temperature structure and dynamic processes can contribute to the N_e distribution.

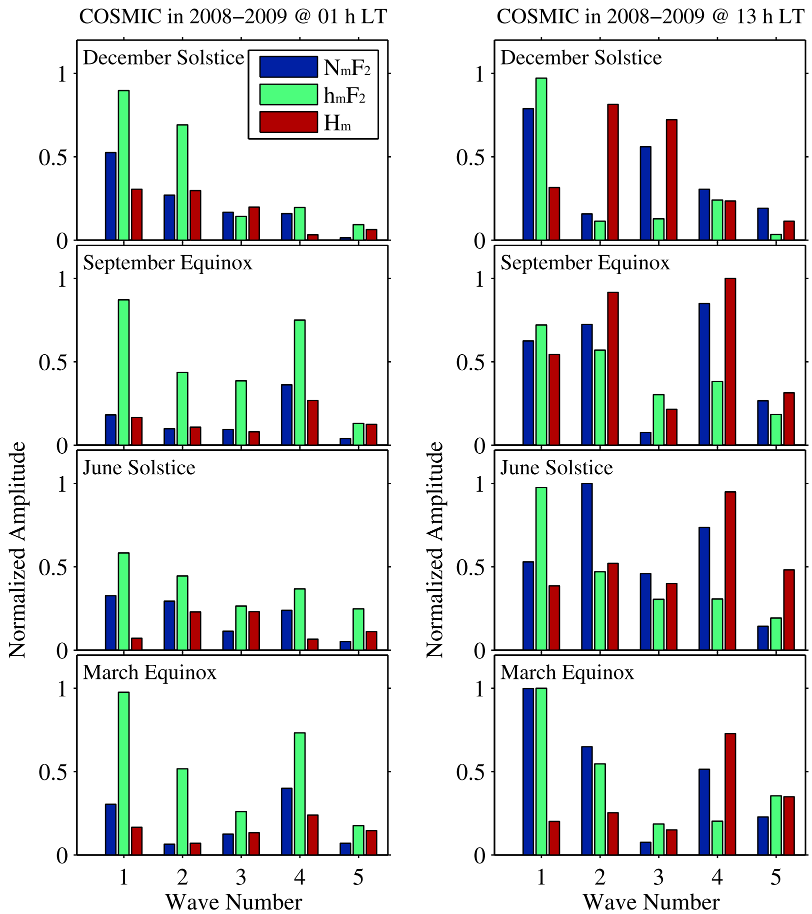

Figure 6. Normalized amplitudes of longitudinal components of wave number 1–5 of N_mF_2, h_mF_2, and H_m, as indicated by the black curves in Figures 3, 4, and 5, respectively, at (left) 0100 LT and (right) 1300 LT in four seasons in 2008–2009.

3.2. Longitudinal Patterns of N_mF_2, h_mF_2, and H_m During 2008–2009

[31] Figures 3, 4, and 5 also demonstrate the longitudinal variations in N_mF_2, h_mF_2 and H_m. An outstanding feature in equatorial regions is wave-like patterns simultaneously existed in the longitudinal variation of all three key parameters. The existence of wave-like features in equatorial H_m is reported for the first time. Several studies have attempted to investigate the longitudinal structures of the scale heights [e.g., *Kutiev et al.*, 2006; *Kutiev and Marinov*, 2007; *Potula et al.*, 2011], but no wave-like longitudinal signature was detected in the scale heights. An exception is *Liu et al.* [2008], which detected the existence of wave-like features in equatorial VSH at 400 km. However, *Potula et al.* [2011] did not find significant longitudinal structures in VSH at 500 km.

[32] In recent years, the wave-like pattern has been detected in the longitudinal variations of nightglow intensity [*Henderson et al.*, 2005; *Immel et al.*, 2006; *Sagawa et al.*, 2005], daytime N_e [e.g., *Lin et al.*, 2007; *Lühr et al.*, 2007], TEC [*Wan et al.*, 2008], plasma drift [*England et al.*, 2006; *Hartman and Heelis*, 2007; *Kil et al.*, 2008; *Ren et al.*, 2009] and VSH [*Liu et al.*, 2008]. It has been recognized that the tilt of the geomagnetic field influences the ionospheric longitudinal dependence [*Hartman and Heelis*, 2007; *Jee et al.*, 2004]. Recent works suggest that this wave-like longitudinal feature is most likely associated with the ionosphere-atmosphere couplings with sources of lower atmospheric origins. The nonmigrating eastward propagating zonal wave number 3 diurnal tide (DE3) and other tide modes are mainly driven by the weather system in tropical atmosphere [*Hagan et al.*, 2007], due to zonal asymmetries in topography, land-sea differences and longitude dependences in absorbing species and nonlinear interactions between the migrating diurnal tides and planetary waves. When they propagate upward to the ionospheric E region [*Oberheide and Forbes*, 2008], the *E* region dynamo interaction with the tides produces electric fields, which are transmitted to F region altitudes by equipotential geomagnetic field lines and modulates longitudinally the plasma along the field lines in the ionospheric *F* region [e.g., *Forbes et al.*, 2008; *Henderson et al.*, 2005; *Immel et al.*, 2006; *Pedatella et al.*, 2008; *Wan et al.*, 2008]. Recent investigations showed that tides can propagate directly up to the thermospheric heights [e.g., *Oberheide and Forbes*, 2008]. It is still under controversy about which one is more important in the ionospheric *F* layer.

[33] The longitude structure is conventionally described by wave numbers. The wave number *k* denotes a longitude variation with zonal wave number *k*. To more explicitly illustrate the longitudinal pattern, we calculate the average values of N_mF_2 and h_mF_2 over the northern crest latitude band (10°–25° northward of the dip equator) and H_m in the

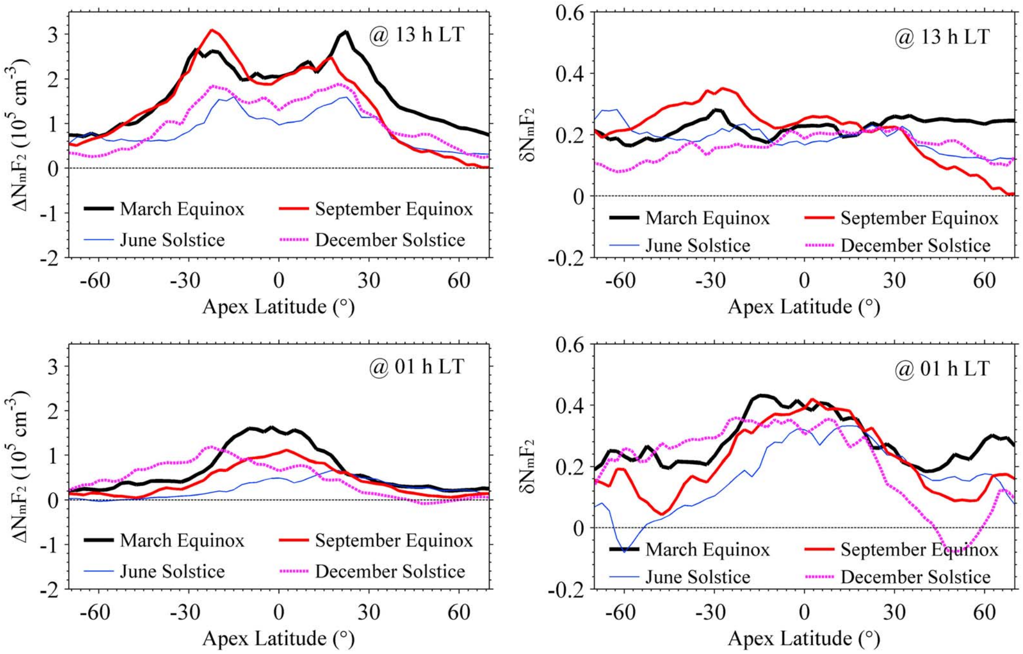

Figure 7. (left) The latitudinal profile of ΔN_mF_2, the difference of longitude-average N_mF_2 for Group B (during periods of 2006, 194–365, 2007, and 2010) from those for Group A (in 2008–2009), in four seasons at 1300 LT and 0100 LT. (right) The latitudinal profile of δN_mF_2, the ratio of ΔN_mF_2 to the longitude-average N_mF_2 for Group B.

equatorial regions (±8° around the dip equator), respectively, which are denoted in black curves in Figures 3, 4, and 5. Furthermore, a spectral analysis is performed on the longitudinal structure of the band-average data for any parameter and season. The maximum value can easily be determined from the wave number 1–5 components in the daytime and nighttime. The amplitudes of the components are normalized by the searched maximum value, respectively. Figure 6 gives histograms of the wave number 1–5 amplitudes of the longitudinal components for the band-average N_mF_2, h_mF_2 and H_m in four seasons.

[34] As shown in Figure 6, in addition to the dominant wave number 1 component, there are other components in the longitudinal structure in the daytime N_mF_2, h_mF_2 and H_m. The band-average N_mF_2 over the northern equatorial anomaly crest is dominated by wave number 2 in June Solstice, wave number 4 in September Equinox, and wave number 3 in December Solstice; h_mF_2 is dominated by wave number 1, along with weaker wave number 4 in December Solstice and wave number 2 in other seasons; and the equatorial H_m displays significant wave number 2 in December Solstice and wave number 4 in other seasons. A larger amplitude wave number 4 in equinoxes is a consistent feature in all three parameters. Daytime wave number 5 shows significant peaks during the June Solstice and March Equinox. In contrast, the longitudinal wave number spectrum is different in the nighttime.

[35] The detected seasonal pattern of longitudinal wave number 4 components is consistent with those in other parameters [*He et al.*, 2010; *Oberheide and Forbes*, 2008; *Ren et al.*, 2009; *Wan et al.*, 2008]. The major contribution to wave number 4 signatures is believed to originate from the DE3 mode excited in the tropical troposphere [*Hagan et al.*, 2007; *Immel et al.*, 2006]. The DE3 mode is observed to dominate over other nonmigrating tidal modes during most of the year, except boreal winter when it is exceeded by the DE2 mode [*Forbes et al.*, 2008; *Pedatella et al.*, 2008]. As a consequence, in Figure 6 the daytime wave number 4 components is weaker than the wave number 3 in December Solstice.

[36] A puzzling question is that the wave-like signature is only found in equatorial H_m. Two possible processes may cause the wave-like longitudinal signature in equatorial H_m. One is the plasma vertical drift, and the other is neutral temperature. Both are effective to equatorial H_m and also show evident wave-like signature in equatorial regions [*Kil et al.*, 2008; *Lühr et al.*, 2007; *Oberheide and Forbes*, 2008]. At present, we have no idea about which one is more important in forming the wave-like signature in equatorial H_m.

3.3. Possible Solar EUV Effect on N_mF_2, h_mF_2, and H_m During Solar Minimum

[37] We organize the data of N_mF_2, h_mF_2 and H_m for the two groups by apex latitude and season. The longitude-average values of N_mF_2, h_mF_2 and H_m at specified local time and apex latitude are evaluated by the similar fitting procedure as described in Section 2. The longitude-average values for group B minusing those for group A is used to determine the differences between the two groups. We use ΔN_mF_2, Δh_mF_2 and ΔH_m to denote the two group difference of N_mF_2, h_mF_2 and H_m, respectively. We further divide ΔN_mF_2, Δh_mF_2 and ΔH_m by N_mF_2, h_mF_2 and H_m of group B, respectively, to determine the relative differences δN_mF_2, δh_mF_2 and δH_m.

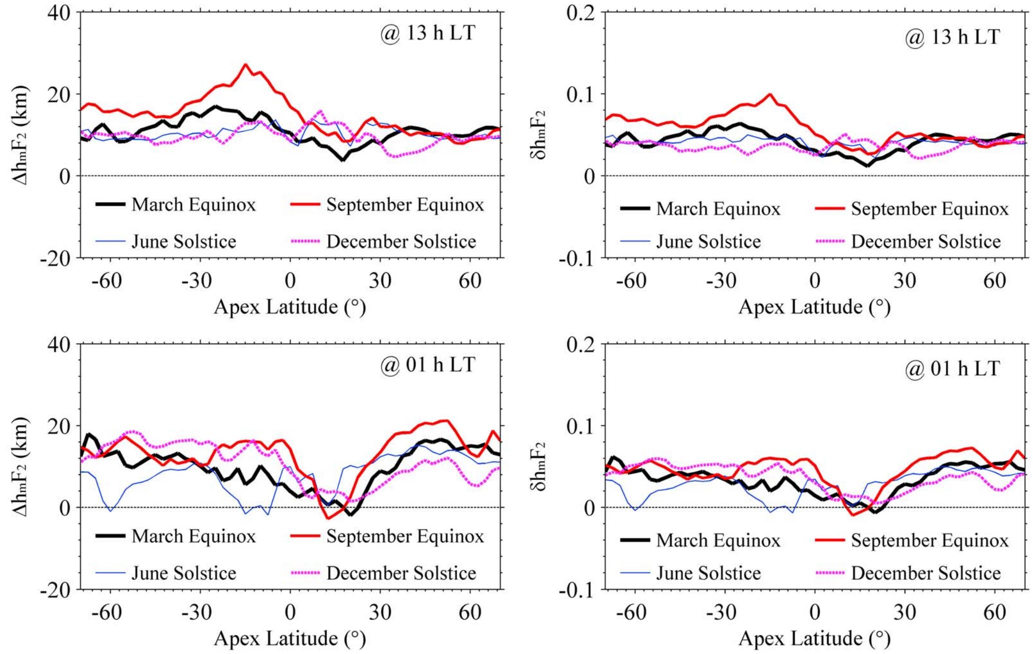

Figure 8. Similar to Figure 7, but for Δh_mF_2 and δh_mF_2. Δh_mF_2 is the difference of longitude-average h_mF_2 for Group B from those for Group A, and δh_mF_2 is the ratio of Δh_mF_2 to the longitude-average h_mF_2 for Group B.

[38] Figures 7, 8, and 9 display the latitudinal profile of ΔN_mF_2, Δh_mF_2 and ΔH_m, respectively, at 13 LT (upper panel) and 01 LT (down panel) during all seasons. The corresponding δN_mF_2, δh_mF_2 and δH_m are also given in the right-hand panels.

[39] From Figures 7, 8, and 9, the following features can be drawn. The values of daytime N_mF_2, h_mF_2 and H_m are generally higher for group B (2006–2007 and 2010) than for group A (2008–2009). It indicates a decrease of about 2×10^4 electrons/cm^3 (minimum value; shown in December solstice) to 3×10^5 electrons/cm^3 (maximum value; in March equinox) in N_mF_2, 5 km (minimum value; in March Equinox) to 28 km (maximum value; in September equinox) in h_mF_2 and 1 km (minimum value; shown in December solstice) to 8 km (maximum value; in September equinox) in H_m during daytime at middle and low latitudes in 2008–2009. A

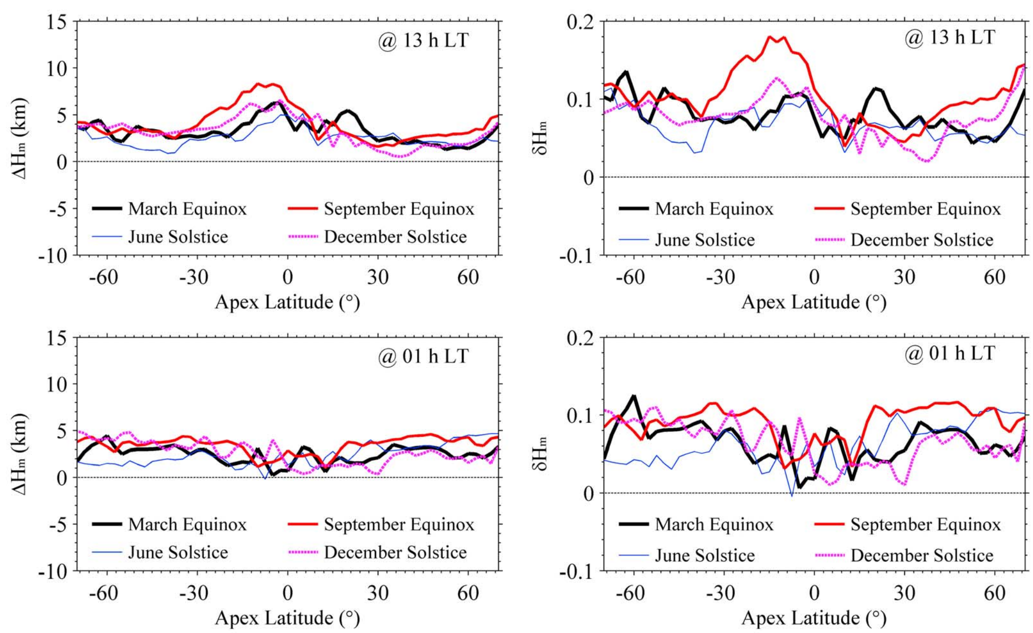

Figure 9. Similar to Figure 7 but for ΔH_m and δH_m. ΔH_m is the difference of longitude-average H_m for Group B from those for Group A, and δH_m is the ratio of ΔH_m to the longitude-average H_m for Group B.

decrease of about 6.6 sfu is also observed in $F_{10.7P}$. This feature is consistent with the reduction pattern in ionosonde N_mF_2, global mean TEC and the ionospheric height in 2008–2009 [*Liu et al.*, 2011b].

[40] Furthermore, the daytime ΔN_mF_2 and ΔH_m are extensively pronounced at low latitudes. With increasing latitude, the two-group differences diminish in both hemispheres. The daytime ΔN_mF_2 is larger during equinoxes than during solstices. In contrast, the nighttime values of ΔN_mF_2 and ΔH_m become smaller than their respective daytime values. Stronger nighttime ΔN_mF_2 presents in March Equinox in equatorial regions and in December Solstice at southern middle latitudes. The nighttime ΔH_m displays a flat latitudinal pattern, showing a weak tendency of larger values at higher latitudes. Regarding Δh_mF_2, it shows weak season and day-night differences and fluctuates around 10 km. At certain latitudes and times, Δh_mF_2 at the nighttime has very small values and even reverses toward negative values in the northern tropical latitudes.

[41] The relative differences δN_mF_2, δh_mF_2 and δH_m show that the 2008–2009 values decrease by about 20% in daytime N_mF_2, 20% to 40% in nighttime N_mF_2, 4% to 8% in daytime h_mF_2, 4% in nighttime h_mF_2 and about 10% in daytime H_m, compared to group B.

[42] One key issue is that, to what extent the reduction in solar EUV can explain the daytime N_mF_2 differences between the two groups. *Liu et al.* [2011a] found that the ionosphere in 2008–2009 changes in a manner that can be predicted by a quadratic fitting of the solar EUV dependency of N_mF_2 and global mean TEC. They verified that the solar EUV reduction is the prevailing contributor to the low electron density in the ionosphere during solar cycle 23/24 minimum.

[43] Indicated from Figure 7 (top), daytime ΔN_mF_2 has higher values in equatorial regions. This feature is generally consistent with the seasonal and latitudinal pattern of the solar EUV sensitivity of N_mF_2. *Liu et al.* [2006] reported a stronger solar EUV sensitivity of N_mF_2 in equatorial regions and in equinoxes (see *Liu et al.* [2006, Figure 5] for details). More specifically, we can estimate the solar EUV sensitivity of N_mF_2 from Figure 7 (top) and the values of $\Delta F_{10.7P}$ in Table 1. The order of magnitude of $dN_mF_2/dF_{10.7P}$ is about 10^3 to 10^4 electrons/cm^3/sfu, which is consistent with the solar EUV sensitivity results of *Liu et al.* [2006]. Accordingly, we suggest that the differences of the daytime ΔN_mF_2 between the two groups can be explained to a great extent by the solar EUV effect.

4. Summary

[44] We made an analysis on the F_2 layer three key parameters, N_mF_2, h_mF_2 and H_m, retrieved from COSMIC N_e profiles to study the ionospheric features and the possible solar EUV effect under the deep solar minimum. The major features are summarized as follows:

[45] 1. Complicated seasonal variations in the COSMIC-observed ionosphere are present at middle and low latitudes under the deep solar minimum. In the daytime, equinoctial asymmetry, nonseasonal and semiannual anomalies are present, while the winter anomaly subsides over most regions; in the nighttime, the Weddell Sea anomaly is a salient feature in all seasons, except during June solstice. Nighttime enhancements can be seen in summer N_mF_2 at northern middle latitudes over a wider range of longitudes (100°E to 150°W).

[46] 2. H_m peaks in the equatorial regions, decrease with latitude in the daytime, and has lowest values at low latitudes in the nighttime. Salient structures include that: (a) higher daytime N_mF_2 shows at middle and high latitudes over the longitude sector from 60°W to 60°E during the March Equinox; (b) compared to other longitudes, higher nighttime h_mF_2 appears over regions around 70°W and higher daytime h_mF_2 and H_m appears over southern middle latitude regions centered at longitude 70°E during December solstice and March Equinox, respectively.

[47] 3. Wave-like longitudinal patterns exist at low latitudes in all three parameters under study, along with diurnal and seasonal nature. In our knowledge, this is the first report on the Hm wave-like structure.

[48] 4. The three parameters under study during 2008–2009 are smaller in the daytime than the rest period of the COSMIC mission. The order of magnitude of $dN_mF_2/dF_{10.7P}$ is estimated to be 10^3 to 10^4 electrons/cm^3/sfu. The seasonal and latitudinal pattern of solar sensitivity of daytime N_mF_2 not only is consistent with our earlier investigation using ionosonde measurements [*Liu et al.*, 2006], but also provides further evidence that the solar EUV reduction can explain the smaller daytime N_mF_2 during 2008–2009 [*Liu et al.*, 2011a]. The nighttime h_mF_2 presents inconsistent features, which requires further investigations.

[49] **Acknowledgments.** We greatly thank the two reviewers for their detailed comments, which greatly improved the manuscript presentation. This study made uses of IRO data from the COSMIC Data Analysis and Archive Center (CDAAC). The F10.7 index is downloaded from the SPIDR Web site (http:/spidr.ngdc.noaa.gov/). This research was supported by the National Natural Science Foundation of China (40725014, 41074112), the China Meteorology Administration grant (GYHY201106011), and the Specialized Research Fund for State Key Laboratories. X. Yue acknowledges support from the U.S. Air Force with funds awarded via the National Science Foundation under Cooperative Agreement AGS-0918398/CSA AGS-0961147.

[50] Robert Lysak thanks the reviewers for their assistance in evaluating this manuscript.

References

Araujo-Pradere, E. A., R. Redmon, M. Fedrizzi, R. Viereck, and T. J. Fuller-Rowell (2011), Some characteristics of the ionospheric behavior during the solar cycle 23–24 minimum [online], *Sol. Phys.*, *270*, doi:10.1007/s11207-011-9728-3.

Balan, N., G. J. Bailey, B. Jenkins, P. B. Rao, and R. J. Moffett (1994), Variations of ionospheric ionization and related solar fluxes during an intense solar cycle, *J. Geophys. Res.*, *99*, 2243–2253, doi:10.1029/93JA02099.

Balan, N., Y. Otsuka, S. Fukao, M. A. Abdu, and G. J. Bailey (2000), Annual variations of the ionosphere: A review based on MU radar observations, *Adv. Space Res.*, *25*, 153–162, doi:10.1016/S0273-1177(99)00913-8.

Bilitza, D., and B. W. Reinisch (2008), International Reference Ionosphere 2007: Improvements and new parameters, *Adv. Space Res.*, *42*, 599–609, doi:10.1016/j.asr.2007.07.048.

Burns, A. G., Z. Zeng, W. Wang, J. Lei, S. C. Solomon, A. D. Richmond, T. L. Killeen, and Y.-H. Kuo (2008), Behavior of the F_2 peak ionosphere over the South Pacific at dusk during quiet summer conditions from COSMIC data, *J. Geophys. Res.*, *113*, A12305, doi:10.1029/2008JA013308.

Chen, Y., L. Liu, and H. Le (2008), Solar activity variations of nighttime ionospheric peak electron density, *J. Geophys. Res.*, *113*, A11306, doi:10.1029/2008JA013114.

Chen, Y., L. Liu, and W. Wan (2011), Does the $F_{10.7}$ index correctly describe solar EUV flux during the deep solar minimum of 2007–2009?, *J. Geophys. Res.*, *116*, A04304, doi:10.1029/2010JA016301.

Duncan, R. A. (1969), *F* region seasonal and magnetic storm behaviour, *J. Atmos. Terr. Phys.*, *31*, 59–70, doi:10.1016/0021-9169(69)90081-6.
Emmert, J. T., J. L. Lean, and J. M. Picone (2010), Record-low thermospheric density during the 2008 solar minimum, *Geophys. Res. Lett.*, *37*, L12102, doi:10.1029/2010GL043671.
England, S. L., S. Maus, T. J. Immel, and S. B. Mende (2006), Longitudinal variation of the *E* region electric fields caused by atmospheric tides, *Geophys. Res. Lett.*, *33*, L21105, doi:10.1029/2006GL027465.
Forbes, J. M., X. Zhang, S. Palo, J. Russell, C. J. Mertens, and M. Mlynczak (2008), Tidal variability in the ionospheric dynamo region, *J. Geophys. Res.*, *113*, A02310, doi:10.1029/2007JA012737.
Gibson, S. E., J. U. Kozyra, G. de Toma, B. A. Emery, T. Onsager, and B. J. Thompson (2009), If the Sun is so quiet, why is the Earth ringing? A comparison of two solar minimum intervals, *J. Geophys. Res.*, *114*, A09105, doi:10.1029/2009JA014342.
Gorney, D. J. (1990), Solar cycle effects on the near-Earth space environment, *Rev. Geophys.*, *28*, 315–336, doi:10.1029/RG028i003p00315.
Hagan, M. E., A. Maute, R. G. Roble, A. D. Richmond, T. J. Immel, and S. L. England (2007), Connections between deep tropical clouds and the Earth's ionosphere, *Geophys. Res. Lett.*, *34*, L20109, doi:10.1029/2007GL030142.
Hartman, W. A., and R. A. Heelis (2007), Longitudinal variations in the equatorial vertical drift in the topside ionosphere, *J. Geophys. Res.*, *112*, A03305, doi:10.1029/2006JA011773.
He, M., L. Liu, W. Wan, B. Ning, B. Zhao, J. Wen, H. Le, and X. Yue (2009), A study of the Weddell Sea Anomaly observed by FORMOSAT-3/COSMIC, *J. Geophys. Res.*, *114*, A12309, doi:10.1029/2009JA014175.
He, M., L. Liu, W. Wan, J. Lei, and B. Zhao (2010), Longitudinal modulation of the O/N_2 column density retrieved from TIMED/GUVI measurement, *Geophys. Res. Lett.*, *37*, L20108, doi:10.1029/2010GL045105.
Heelis, R. A., W. R. Coley, A. G. Burrell, M. R. Hairston, G. D. Earle, M. D. Perdue, R. A. Power, L. L. Harmon, B. J. Holt, and C. R. Lippincott (2009), Behavior of the O+/H+ transition height during the extreme solar minimum of 2008, *Geophys. Res. Lett.*, *36*, L00C03, doi:10.1029/2009GL038652.
Henderson, S. B., C. M. Swenson, A. B. Christensen, and L. J. Paxton (2005), Morphology of the equatorial anomaly and equatorial plasma bubbles using image subspace analysis of Global Ultraviolet Imager data, *J. Geophys. Res.*, *110*, A11306, doi:10.1029/2005JA011080.
Horvath, I., and E. A. Essex (2003), The Weddell Sea anomaly observed with the TOPEX satellite data, *J. Atmos. Sol. Terr. Phys.*, *65*, 693–706, doi:10.1016/S1364-6826(03)00083-X.
Immel, T. J., E. Sagawa, S. L. England, S. B. Henderson, M. E. Hgan, S. B. Mende, H. U. Frey, C. M. Swenson, and L. J. Paxton (2006), Control of equatorial ionospheric morphology by atmospheric tides, *Geophys. Res. Lett.*, *33*, L15108, doi:10.1029/2006GL026161.
Jee, G., R. W. Schunk, and L. Scherliess (2004), Analysis of TEC data from the TOPEX/Poseidon mission, *J. Geophys. Res.*, *109*, A01301, doi:10.1029/2003JA010058.
Kawamura, S., N. Balan, Y. Otsuka, and S. Fukao (2002), Annual and semiannual variations of the midlatitude ionosphere under low solar activity, *J. Geophys. Res.*, *107*(A8), 1166, doi:10.1029/2001JA000267.
Kil, H., E. R. Talaat, S.-J. Oh, L. J. Paxton, S. L. England, and S.-J. Su (2008), Wave structures of the plasma density and vertical E × B drift in low-latitude F region, *J. Geophys. Res.*, *113*, A09312, doi:10.1029/2008JA013106.
Kutiev, I., and P. Marinov (2007), Topside sounder model of scale height and transition height characteristics of the ionosphere, *Adv. Space Res.*, *39*, 759–766, doi:10.1016/j.asr.2006.06.013.
Kutiev, I. S., P. G. Marinov, and S. Watanabe (2006), Model of topside ionosphere scale height based on topside sounder data, *Adv. Space Res.*, *37*, 943–950, doi:10.1016/j.asr.2005.11.021.
Lean, J. L., J. T. Emmert, J. M. Picone, and R. R. Meier (2011), Global and regional trends in ionospheric total electron content, *J. Geophys. Res.*, *116*, A00H04, doi:10.1029/2010JA016378.
Lin, C. H., C. C. Hsiao, J. Y. Liu, and C. H. Liu (2007), Longitudinal structure of the equatorial ionosphere: Time evolution of the four-peaked EIA structure, *J. Geophys. Res.*, *112*, A12305, doi:10.1029/2007JA012455.
Liu, L., and Y. Chen (2009), Statistical analysis on the solar activity variations of the TEC derived at JPL from global GPS observations, *J. Geophys. Res.*, *114*, A10311, doi:10.1029/2009JA014533.
Liu, L., W. Wan, B. Ning, O. M. Pirog, and V. I. Kurkin (2006), Solar activity variations of the ionospheric peak electron density, *J. Geophys. Res.*, *111*, A08304, doi:10.1029/2006JA011598.
Liu, L., H. Le, W. Wan, M. P. Sulzer, J. Lei, and M.-L. Zhang (2007), An analysis of the scale heights in the lower topside ionosphere based on the Arecibo incoherent scatter radar measurements, *J. Geophys. Res.*, *112*, A06307, doi:10.1029/2007JA012250.
Liu, L., M. He, W. Wan, and M.-L. Zhang (2008), Topside ionospheric scale heights retrieved from Constellation Observing System for Meteorology, Ionosphere, and Climate radio occultation measurements, *J. Geophys. Res.*, *113*, A10304, doi:10.1029/2008JA013490.
Liu, L., W. Wan, B. Ning, and M.-L. Zhang (2009a), Climatology of the mean TEC derived from GPS Global Ionospheric Maps, *J. Geophys. Res.*, *114*, A06308, doi:10.1029/2009JA014244.
Liu, L., B. Zhao, W. Wan, B. Ning, M.-L. Zhang, and M. He (2009b), Seasonal variations of the ionospheric electron densities retrieved from Constellation Observing System for Meteorology, Ionosphere, and Climate mission radio occultation measurements, *J. Geophys. Res.*, *114*, A02302, doi:10.1029/2008JA013819.
Liu, L., M. He, X. Yue, B. Ning, and W. Wan (2010), The ionosphere around equinoxes during low solar activity, *J. Geophys. Res.*, *115*, A09307, doi:10.1029/2010JA015318.
Liu, L., Y. Chen, H. Le, V. I. Kurkin, N. M. Polekh, and C. C. Lee (2011a), The ionosphere under prolonged extremely low solar activity, *J. Geophys. Res.*, *116*, A04320, doi:10.1029/2010JA016296.
Liu, L., W. Wan, Y. Chen, and H. Le (2011b), Solar activity effects of the ionosphere: A brief review, *Chin. Sci. Bull.*, *56*, 1202–1211, doi:10.1007/s11434-010-4226-9.
Luan, X., and S. C. Solomon (2008), Meridional winds derived from COSMIC radio occultation measurements, *J. Geophys. Res.*, *113*, A08302, doi:10.1029/2008JA013089.
Luan, X., W. Wang, A. Burns, S. C. Solomon, and J. Lei (2008), Midlatitude nighttime enhancement in *F* region electron density from global COSMIC measurements under solar minimum winter condition, *J. Geophys. Res.*, *113*, A09319, doi:10.1029/2008JA013063.
Lühr, H., and C. Xiong (2010), The IRI-2007 model overestimates electron density during the 23/24 solar minimum, *Geophys. Res. Lett.*, *37*, L23101, doi:10.1029/2010GL045430.
Lühr, H., K. Häusler, and C. Stolle (2007), Longitudinal variation of *F* region electron density and thermospheric zonal wind caused by atmospheric tides, *Geophys. Res. Lett.*, *34*, L16102, doi:10.1029/2007GL030639.
Mayr, H. G., and K. K. Mahajan (1971), Seasonal variation in the F2 region, *J. Geophys. Res.*, *76*, 1017–1027, doi:10.1029/JA076i004p01017.
Mendillo, M., C. Huang, X. Pi, H. Rishbeth, and R. Meier (2005), The global ionospheric asymmetry in total electron content, *J. Atmos. Sol. Terr. Phys.*, *67*, 1377–1387, doi:10.1016/j.jastp.2005.06.021.
Moffett, R. J. (1979), The equatorial anomaly in the electron distribution of the terrestrial *F* region, *Fundam. Cosmic Phys.*, *4*, 313–391.
Oberheide, J., and J. M. Forbes (2008), Tidal propagation of deep tropical cloud signatures into the thermosphere from TIMED observations, *Geophys. Res. Lett.*, *35*, L04816, doi:10.1029/2007GL032397.
Pedatella, N. M., J. M. Forbes, and J. Oberheide (2008), Intra-annual variability of the low-latitude ionosphere due to nonmigrating tides, *Geophys. Res. Lett.*, *35*, L18104, doi:10.1029/2008GL035332.
Penndorf, R. (1965), The average ionospheric conditions over the Antarctic, in *Geomagnetism and Aeronomy*, *Antarct. Res. Ser*, vol. 4, edited by A. H. Waynick, pp. 1–45, AGU, Washington, D. C.
Potula, B. S., Y.-H. Chu, G. Uma, H.-P. Hsia, and K.-H. Wu (2011), A global comparative study on the ionospheric measurements between COSMIC radio occultation technique and IRI model, *J. Geophys. Res.*, *116*, A02310, doi:10.1029/2010JA015814.
Ren, Z., W. Wan, L. Liu, and J. Xiong (2009), Intra-annual variation of wavenumber-4 structure of vertical E × B drifts in the equatorial ionosphere seen from ROCSAT-1, *J. Geophys. Res.*, *114*, A05308, doi:10.1029/2009JA014060.
Richards, P. G., J. A. Fennelly, and D. G. Torr (1994), EUVAC: A solar EUV flux model for aeronomic calculations, *J. Geophys. Res.*, *99*, 8981–8992, doi:10.1029/94JA00518.
Rishbeth, H. (1998), How the thermospheric circulation affects the ionosphere, *J. Atmos. Sol. Terr. Phys.*, *60*, 1385–1402, doi:10.1016/S1364-6826(98)00062-5.
Rishbeth, H., and O. K. Garriott (1969), *Introduction to Ionospheric Physics*, 331 pp., Academic, San Diego, Calif.
Russell, C. T., J. G. Luhmann, and L. K. Jian (2010), How unprecedented a solar minimum?, *Rev. Geophys.*, *48*, RG2004, doi:10.1029/2009RG000316.
Rüster, R., and J. W. King (1973), Atmospheric composition changes and the *F*2-layer seasonal anomaly, *J. Atmos. Terr. Phys.*, *35*, 1317–1322, doi:10.1016/0021-9169(73)90164-5.
Sagawa, E., T. J. Immel, H. U. Frey, and S. B. Mende (2005), Longitudinal structure of equatorial anomaly in the nighttime ionosphere observed by IMAGE/FUV, *J. Geophys. Res.*, *110*, A11302, doi:10.1029/2004JA010848.
Smithtro, C. G., and J. J. Sojka (2005), Behavior of the ionosphere and thermosphere subject to extreme solar cycle conditions, *J. Geophys. Res.*, *110*, A08306, doi:10.1029/2004JA010782.

Solomon, S. C., T. N. Woods, L. V. Didkovsky, J. T. Emmert, and L. Qian (2010), Anomalously low solar extreme-ultraviolet irradiance and thermospheric density during solar minimum, *Geophys. Res. Lett.*, *37*, L16103, doi:10.1029/2010GL044468.

Torr, M. R., and D. G. Torr (1973), The seasonal behaviour of the *F*2-layer of the ionosphere, *J. Atmos. Terr. Phys.*, *35*, 2237–2251, doi:10.1016/0021-9169(73)90140-2.

Wan, W., L. Liu, X. Pi, M. Zhang, B. Ning, J. Xiong, and F. Ding (2008), Wavenumber-4 patterns of the total electron content over the low latitude ionosphere, *Geophys. Res. Lett.*, *35*, L12104, doi:10.1029/2008GL033755.

Wright, J. W. (1963), The *F* region seasonal anomaly, *J. Geophys. Res.*, *68*, 4379–4381.

Yue, X., W. S. Schreiner, J. Lei, S. V. Sokolovskiy, C. Rocken, D. C. Hunt, and Y.-H. Kuo (2010a), Error analysis of Abel retrieved electron density profiles from radio occultation measurements, *Ann. Geophys.*, *28*, 217–222, doi:10.5194/angeo-28-217-2010.

Yue, X., W. S. Schreiner, J. Lei, C. Rocken, D. C. Hunt, Y.-H. Kuo, and W. Wan (2010b), Global ionospheric response observed by COSMIC satellites during the January 2009 stratospheric sudden warming event, *J. Geophys. Res.*, *115*, A00G09, doi:10.1029/2010JA015466.

Zeng, Z., A. Burns, W. Wang, J. Lei, S. Solomon, S. Syndergaard, L. Qian, and Y. Kuo (2008), Ionospheric annual asymmetry observed by the COSMIC radio occultation measurements and simulated by the TIEGCM, *J. Geophys. Res.*, *113*, A07305, doi:10.1029/2007JA012897.

Y. Chen, M. He, H. Le, L. Liu, and W. Wan, Beijing National Observatory of Space Environment, Institute of Geology and Geophysics, Chinese Academy of Sciences, Beijing 100029, China. (liul@mail.iggcas.ac.cn)

X. Yue, COSMIC Program Office, University Corporation for Atmospheric Research, Boulder, CO 80020, USA.